High spin band structures in doubly odd ^{194}Tl

H. Pai, G. Mukherjee,* S. Bhattacharyya, M. R. Gohil, T. Bhattacharjee, and C. Bhattacharya
Variable Energy Cyclotron Centre, 1/AF Bidhannagar, Kolkata 700064, India

R. Palit, S. Saha, J. Sethi, T. Trivedi, Shital Thakur, B. S. Naidu, S. K. Jadav, and R. Donthi
Department of Nuclear and Atomic Physics, Tata Institute of Fundamental Research, Mumbai 400005, India

A. Goswami
Saha Institute of Nuclear Physics, 1/AF Bidhannagar, Kolkata 700064, India

S. Chanda
Fakir Chand College, Diamond Harbour, West Bengal, India
(Received 29 September 2011; published 12 June 2012)

The high spin states in the odd-odd ^{194}Tl nucleus have been studied by populating them using the ^{185,187}Re(^{13}C, xn) reactions at a beam energy of 75 MeV. A γ-γ coincidence measurement has been performed using the INGA array with a digital data acquisition system to record the time-stamped data. Definite spin-parity assignment of the levels was made from the DCO ratio and the IPDCO ratio measurements. The level scheme of ^{194}Tl has been extended up to 4.1 MeV in excitation energy and includes 19 new γ-ray transitions. The $\pi h_{9/2} \otimes \nu i_{13/2}$ band, in the neighboring odd-odd Tl isotopes, show very similar properties in both experimental observables and calculated shapes. Two new band structures, with six-quasiparticle configuration, have been observed in ^{194}Tl. One of these bands has the characteristics of a magnetic rotational band. Cranked shell model calculations, using a deformed Woods-Saxon potential, have been performed to obtain the total Routhian surfaces in order to study the shapes of the bands and the band crossing in ^{194}Tl. A semiclassical formalism has been used to describe the magnetic rotational band.

DOI: 10.1103/PhysRevC.85.064313 PACS number(s): 21.10.Re, 23.20.Lv, 23.20.En, 21.60.Cs

I. INTRODUCTION

The thallium nuclei, with proton number $Z = 81$, are situated in a transition region between the deformed prolate rare-earth nuclei and the spherical lead nuclei at $Z = 82$. The proton Fermi level in Tl lies below the $Z = 82$ shell closure and near the $2s_{1/2}$ orbtal. The ground-state spin-parity of the heavier odd-A thalium isotopes are, accordingly, $1/2^+$ [1–3]. However, the intruder $9/2^-[505]$ and $1/2^-[541]$ Nilsson states, originating from the $\pi h_{9/2}$ orbital above $Z = 82$, are also available near the Fermi surface for oblate and prolate deformations, respectively. The experimental evidence comes from the observation of a low-lying $9/2^-$ isomeric state and strongly coupled rotational bands built on this in the odd-A thalium isotopes [4–8]. The neutron Fermi surface for the Tl and Hg isotopes in the $A \sim 190$ region lie near the top of the $1i_{13/2}$ orbital and decoupled bands with this configuration have been identified in odd-A Hg ($Z = 80$) isotopes in this region [9,10]. Therefore, in even-mass Tl isotopes in this region, collective rotational bands based on the $\pi h_{9/2} \otimes \nu i_{13/2}$ configuration are expected. Such bands have been experimentally observed in a few odd-odd Tl isotopes [11–17]. But, in most of the cases, there are ambiguities on level energies, spins, and parities. Recently, experimental studies on the structures of ^{190}Tl [11] and ^{198}Tl [17] have been reported with definite spin-parity assignment of the $\pi h_{9/2} \otimes \nu i_{13/2}$ band. In ^{190}Tl, this band, which shows a low-spin signature inversion, was reported to have an oblate structure, whereas, in ^{198}Tl, the possible chiral structure associated with this band was interpreted with a triaxial deformation. Therefore, in order to understand the possible transition from oblate to triaxial shape induced by the change in the neutron Fermi surface of Tl nuclei, it is important to characterize the $\pi h_{9/2} \otimes \nu i_{13/2}$ band systematically in an isotopic chain. But the high spin data on the other odd-odd Tl nuclei are scarce. Moreover, both the protons and the neutrons occupy high-j orbitals, so different kinds of collective and single-particle excitations, such as magnetic rotation, are expected. Although several magnetic rotational bands have been observed in Pb and Hg nuclei in this region [18,19], no such bands are reported for Tl isotopes.

Knowledge of high spin states in ^{194}Tl was very limited prior to the present work; although several superdeformed bands have been reported for this nucleus by Azaiez *et al.*, these bands were not connected with the normal deformed bands [20,21]. The normal deformed high spin states in ^{194}Tl were studied by Kreiner *et al.* [13] and a level scheme was obtained using two Ge(Li) detectors. Although indication of rotational bands based on the $\pi h_{9/2} \otimes \nu i_{13/2}$ configuration was reported in that work, no definite spin-parity assignments could be made. Possible observation of chiral partner bands in ^{194}Tl has been claimed recently [22] but no such level scheme has been reported yet. In this work, we have studied the γ-ray spectroscopy of ^{194}Tl with the aim, in particular, of comparing the band structures in odd-odd Tl isotopes and of searching for a possible magnetic rotational band.

*Corresponding author: gopal@vecc.gov.in

II. EXPERIMENTAL METHOD AND DATA ANALYSIS

The γ-ray spectroscopy of ^{194}Tl has been studied at the 14-UD BARC-TIFR Pelletron at Mumbai, India, using the Indian National Gamma Array (INGA). INGA consisted of 15 clover HPGe detectors with BGO anti-Compton shields at the time of the experiment. The excited states of ^{194}Tl were populated by fusion-evaporation reactions ^{185,187}Re(^{13}C, xn)^{194}Tl at a beam energy of 75 MeV. The target was a thick (18.5 mg/cm^2) natural rhenium target. The recoils were stopped inside the target. The isotopic ratio of ^{185}Re and ^{187}Re in natural rhenium is 37:63. According to PACE-IV calculations, the 4n and 5n channels are the dominant ones at the beam energies encompassed inside the target in this experiment. The beam energy at the exit of the target was calculated to be below the Coulomb barrier. The clover detectors were arranged in six angles with two clovers each at $\pm 40^\circ$ and $\pm 65^\circ$ while four clovers were at 90° and three were at -23° angles. The average count rate in each crystal was limited to $\sim$4000/s. The clover detectors were calibrated for γ-ray energies and efficiencies by using ^{133}Ba and ^{152}Eu radioactive sources.

Recently, a digital data acquisition (DDAQ) system, based on Pixie-16 modules developed by XIA LLC [23], has been adopted for INGA. This system has provision for the digitization of 96 channels of 24 clover detectors (the maximum number of clover detectors that can be put in INGA) with a sampling rate of 100 MHz. This DDAQ system was used in the present experiment for the data collection. Time-stamped data were collected when at least two (Compton-suppressed) clovers were fired in coincidence. A time window of 150 ns was set for this coincidence between the fast triggers of individual channels, and the coincidence trigger was kept open for 1.5 μs. The BGO signals from the anti-Compton shields of the respective clovers were used for vetoing the individual channels. The detailed description of the DDAQ has been given in Refs. [24,25].

The data-sorting routine Multi pARameter time-stamped based COincidence Search (MARCOS) program, developed at TIFR, sorts the time-stamped data to generate a E_γ-E_γ matrix and a E_γ-E_γ-E_γ cube in a RADWARE-compatible format for further analysis. To construct these, a coincidence time window of 400 ns was selected. RADWARE software [26] was used for the analysis of the matrix and the cube. The E_γ-E_γ matrix contained about 2.4 $\times$ 10^9 coincidence events. To construct the level scheme of ^{194}Tl, the coincidence and the intensity relations of the γ rays were used. Gates were put on the known γ-ray transitions for determining the coincidence relations. Single- and double-gated γ-ray spectra from the E_γ-E_γ matrix and E_γ-E_γ-E_γ cube are shown in Figs. 1 and 2, respectively. The relevance of these spectra in the level scheme will be discussed in the next section. The intensities of the γ rays were obtained from the E_γ-E_γ matrix using a single-gated spectrum.

The multipolarities of the γ-ray transitions have been determined from an angular correlation analysis using the method of directional correlation from the oriented states (DCO) ratio, following the prescriptions of Krämer-Flecken *et al.* [27]. For the DCO ratio analysis, the coincidence events were sorted into an asymmetry matrix with data from the 90°

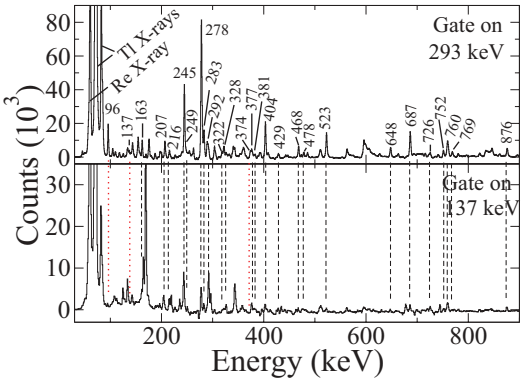

FIG. 1. (Color online) Coincidence spectra by gating on 293-keV (top) and 137-keV (bottom) γ transitions. The unmarked peaks are the contaminants.

detectors (θ_1) on one axis and data from the -23° detectors (θ_2) on the other axis. The DCO ratios (for the γ ray γ_1, gated by a γ ray γ_2 of known multipolarity) are obtained from the intensities of the γ rays (I_γ), at two angles θ_1 and θ_2, as

$$R_{\rm DCO} = \frac{I_{\gamma_1} \text{ at } \theta_1, \text{ gated by } \gamma_2 \text{ at } \theta_2}{I_{\gamma_1} \text{ at } \theta_2, \text{ gated by } \gamma_2 \text{ at } \theta_1}. \quad (1)$$

By putting gates on the transitions with known multipolarity along the two axes of the above matrix, the DCO ratios are obtained for each γ ray. For stretched transitions, the value of $R_{\rm DCO}$ would be close to unity for the same multipolarity of γ_1 and γ_2. For different multipolarities and mixed transition, the value of $R_{\rm DCO}$ depends on the detector angles (θ_1 and θ_2) and the mixing ratio (δ). The validity of the $R_{\rm DCO}$ measurements was checked with the known transitions in ^{194}Tl and with the calculated values. In the present geometry, the calculated value of $R_{\rm DCO}$ [28] for a pure dipole transition gated by a stretched quadrupole transition is 1.65 while for a quadrupole transition gated by a pure dipole, the calculated value is 0.61. These compare well with the experimental values of 1.69(3) and 0.58(2), respectively, for the known pure dipole (293-keV, $E1$) and stretched quadrupole (687-keV, $E2$) transitions.

The use of clover HPGe detectors allowed us to assign definite parities to the excited states from the measurement of the integrated polarization asymmetry (IPDCO) ratio, as described in [29,30], from the parallel and perpendicular scattering of a γ-ray photon inside the detector medium. The IPDCO ratio measurement gives a qualitative idea about the type of transition (electric or magnetic). The IPDCO asymmetry parameters have been deduced using the relation

$$\Delta_{\rm IPDCO} = \frac{a(E_\gamma)N_\perp - N_\parallel}{a(E_\gamma)N_\perp + N_\parallel}, \quad (2)$$

where $N_\parallel$ and $N_\perp$ are the counts for the actual Compton-scattered γ rays in the planes parallel and perpendicular to the reaction plane. The correction due to the asymmetry in the array and response of the clover segments, defined by $a(E_\gamma) = \frac{N_\parallel}{N_\perp}$, was checked using ^{152}Eu and ^{133}Ba sources and was found to be 1.004(1), which is close to unity, as expected.

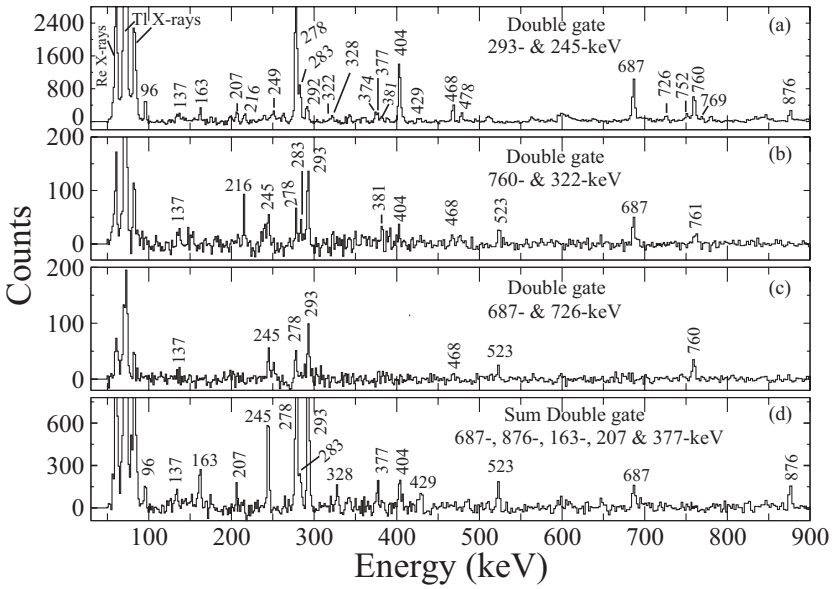

FIG. 2. Coincidence spectra corresponding to double gates of (a) 293 and 245 keV, (b) 760 and 322 keV, and (c) 687 and 726 keV and (d) a sum of double-gated spectra corresponding to the transitions in ^{194}Tl.

The data of $a(E_\gamma)$ and the fitting are shown in Fig. 3. By using the fitted parameter $a(E_\gamma)$, the $\Delta_{\rm IPDCO}$ of the γ rays in ^{194}Tl have been determined. A positive value of $\Delta_{\rm IPDCO}$ indicates an electric-type transition whereas a negative value favors a magnetic-type transition. $\Delta_{\rm IPDCO}$ values could not be measured for the low-energy and weaker transitions. The low-energy cutoff for the polarization measurement was about 200 keV in this work. The validity of the method of the IPDCO measurements was confirmed from the known transitions in ^{194}Tl. The parallel ($N_\parallel$) and perpendicular [$a(E_\gamma)\,N_\perp$] counts for two γ rays in ^{194}Tl are shown in Fig. 4. It shows that the magnetic (404-keV) and the electric (687-keV) transitions can easily be identified.

III. EXPERIMENTAL RESULTS

The level scheme of ^{194}Tl, as obtained in the present work, is shown in Fig. 5. A total of 19 new γ rays have been found and placed in the level scheme. They are marked with asterisks (*) in the level scheme of Fig. 5. The deduced excitation energy, spin, and parity of the excited levels and the multipolarity of the γ rays, together with the other relevant information concerning their placement in the proposed level scheme of ^{194}Tl, are summarized in Table I.

The 2^- ground state (not shown in Fig. 5) and the 7^+ isomeric state ($T_{1/2} = 32.8$ min) were known in ^{194}Tl from β-decay studies [31]. No γ-ray transition was known to decay from the isomeric state. The excitation energy of this state was also not known. Both the ground and the isomeric states decay by electron capture decay. The excitation energies of the states, in the level scheme presented in Fig. 5, have been given with respect to the 7^+ isomeric state, as was presented in Refs. [11,17] for ^{190,198}Tl. In the present work, the level scheme of ^{194}Tl has been extended up to an excitation energy of ~4.1 MeV and $(21^-)\hbar$ spin and is a much improved one compared to the previously known level scheme reported in Ref. [13]. The proposed level scheme is based on the following arguments.

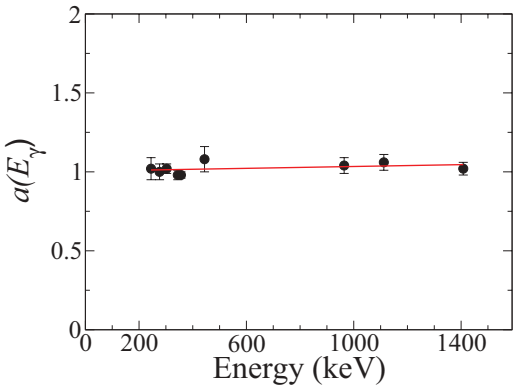

FIG. 3. (Color online) The asymmetry correction factor $a(E_\gamma)$ at different γ energies from ^{152}Eu and ^{133}Ba sources. The solid line corresponds to a linear fit of the data.

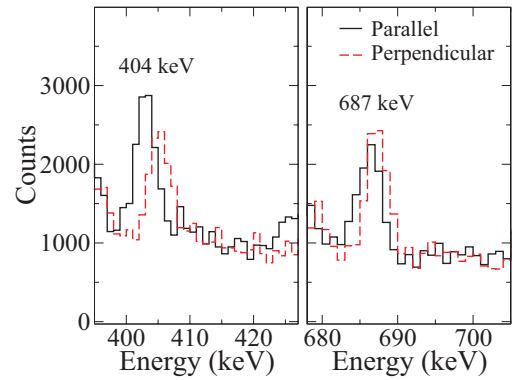

FIG. 4. (Color online) The perpendicular (dashed) and parallel (solid) components of the two γ rays in ^{194}Tl, obtained from the IPDCO analysis in the present work. The perpendicular component has been shifted in energy for clarity. The transition at 404 keV is a known magnetic type whereas the 687-keV transition is a known electric type.

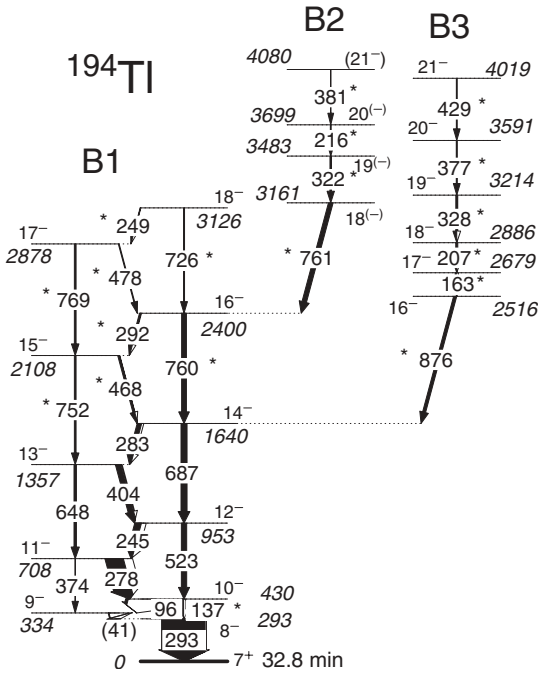

FIG. 5. Level scheme of ^{194}Tl obtained from the present work. The excitation energies are given with respect to the 7^+ isomeric state. The new γ rays are indicated by asterisks.

A 293-keV γ ray from the 8^- to the 7^+ isomeric state in ^{194}Tl was known, from the systematics of the Tl isotopes, to be a hindered $E1$ transition. The DCO ratio and the positive value of the IPDCO ratio, obtained in the present work, confirm this assignment. A 137-keV γ ray has been observed in the present work which is in coincidence with the known 293-keV transition from the 8^- to the 7^+ state, as can be seen from Fig. 1 (top panel). A spectrum gated by this 137-keV γ line, shown in the bottom panel of Fig. 1, shows all the γ rays in ^{194}Tl present in the 293-keV gated spectrum, except for the lines at 96 and 374 keV. This γ ray is also observed in the double-gated spectra shown in Fig. 2. This clearly indicates that there is a 137 keV γ-ray transition above the 293-keV transition and in parallel to the 96-keV transition. It establishes the 334-keV level as the previously unknown energy upon which the rest of the band is built. The DCO ratio for the 137-keV γ ray has been measured in this work gated by the 687-keV γ ray, which was known to be a quadrupole ($E2$) transition [13]. The value of this ratio comes out to be close to unity (see Table I), indicating the stretched quadrupole nature of the 137-keV transition. Although the energy of this γ ray is too low for the IPDCO measurement, the $M2$ assignment for this low-energy transition may be completely ruled out from the lifetime consideration. Therefore, by considering the 137-keV γ ray as an $E2$ transition, the spin and parity of the 430-keV level has been assigned, in this work, as 10^-. The 374-keV γ ray was reported as a tentative one in Ref. [13]. The double-gated spectrum of 293 and 245 keV shown in Fig. 2(a) has a peak at 374 keV, which confirms its placement. The $E2$ nature of this transition is also evident from the measured R_{DCO} value (close to unity) gated by a known $E2$ transition. The placement of the above γ rays indicates that there should be a 41-keV transition from the 9^- to the 8^- state. This low-energy highly converted ($\alpha \sim 200$) transition has not been observed in this work as our experimental setup was not suited to detect such transitions.

It can be seen from Fig. 2(a) that all the γ rays reported in Ref. [13] have been observed in the present work up to the 1640-keV state. However, the 748.6-, 741.9-, 458.6-, and 289.4- keV γ rays, reported in Ref. [13] and placed above the 1640-keV state, were not observed. Instead, we have observed a cascade of 468-, 292-, 478-, and 249-keV $M1 + E2$ γ rays above the 1640-keV state along with the crossover $E2$ transitions. These γ rays have been placed above the 687-keV γ ray in band B1 as they satisfy the corresponding coincidence relations. It may be pointed out that a more efficient experimental setup was used in the present work than in the earlier work. With the observation of these transitions, the negative-parity ground band B1 has been extended up to an excitation energy of 3.13 MeV and a spin of $18\hbar$.

We have also observed two other bandlike structures B2 and B3 in ^{194}Tl. They are placed above the 16^- and the 14^- states of band B1, respectively. The γ lines belonging to these bands can be seen in the single- and double-gated spectra shown in Fig. 1 and Fig. 2(a). The spectrum in Fig. 2(b) (double gate on 760 and 322 keV) shows the γ rays belonging to band B2. The spectrum also shows the 761-keV γ ray, indicating its double placement. The 687-keV line is observed in this spectrum but not the 726-keV line. The 216- and the 381-keV γ rays, belonging to this band, are also observed in this spectrum. The double-gated spectrum of 687 and 726 keV [Fig. 2(c)] shows the 760-keV line, slightly lower in energy than the one in Fig. 2(b). Therefore, the higher energy transition (i.e., 761 keV) of the 760-keV doublet has been assigned as the linking transition between bands B2 and B1. Therefore, the lower energy transition (i.e., 760 keV) of the doublet corresponds to the member of band B1. The 216-, 322-, and 381-keV γ rays are not observed in the spectrum of Fig. 2(c) and hence they form the members of band B2.

To get an unambiguous value for the DCO ratios for the 760- and 761-keV transitions, the gating transitions were selected carefully. The DCO ratio values of the doublet cannot be distinguished for any choice of a pure $E2$ gating transition below the 14^- level. However, in the 468-keV gate, the 760-keV transition (in band B1) would be absent and an unambiguous value of the DCO ratio can be obtained for the 761-keV linking transition. The 468-keV transition has been found to be an $M1$ transition with very little or no $E2$ admixture from the negative value of its IPDCO ratio. So, the 468-keV dipole transition was chosen to obtain the DCO ratio of the 761-keV linking transition and, similarly, the 726-keV quadrupole transition has been chosen as the gating transition to obtain the DCO ratio value of the 760-keV in-band transition. The DCO ratios of the 760- and 761-keV transitions, obtained in this way, suggest that both of them are quadrupole transitions. The IPDCO ratio, measured for the in-band 760-keV transition, clearly suggests that it is an $E2$ transition. The IPDCO ratio could not be obtained for the 761-keV transition and an $E2$ character for this linking transition has

TABLE I. Energy of the γ rays (E_γ) observed in the present work along with the energy of the de-exciting levels (E_i), spin and parity of the initial and final states ($J_i^\pi \rightarrow J_f^\pi$), intensity of the γ rays (I_γ), experimental values of the DCO ($R_{\rm DCO}$) and the IPDCO ($\Delta_{\rm IPDCO}$) ratios, and the deduced multipolarity of the γ rays.

E_γ (keV)	E_i (keV)	$J_i^\pi \rightarrow J_f^\pi$	I_γ[a]	$R_{\rm DCO}$	$\Delta_{\rm IPDCO}$	Deduced multipolarity
96.1(1)	430.0	$10^- \rightarrow 9^-$	5.95(9)	1.59(17)[b]	–	$M1+E2$
136.9(2)	430.0	$10^- \rightarrow 8^-$	2.73(6)	0.96(14)[b]	–	$E2$
162.5(1)	2679.0	$17^- \rightarrow 16^-$	2.24(4)	1.67(20)[b]	–	$M1$
207.1(1)	2886.1	$18^- \rightarrow 17^-$	2.16(4)	1.72(18)[b]	–	$M1$
215.5(2)	3698.6	$20^{(-)} \rightarrow 19^{(-)}$	1.40(2)	1.51(14)[b]	–	$M1+E2$
244.9(1)	953.2	$12^- \rightarrow 11^-$	14.92(41)	1.61(5)[b]	−0.10(2)	$M1(+E2)$
248.6(3)	3125.5	$18^- \rightarrow 17^-$	0.94(2)	1.64(19)[b]	−0.13(10)	$M1+E2$
278.4(1)	708.4	$11^- \rightarrow 10^-$	41.86(62)	1.62(3)[b]	−0.14(1)	$M1(+E2)$
283.2(1)	1640.0	$14^- \rightarrow 13^-$	10.00(15)	1.85(14)[c]	−0.24(4)	$M1(+E2)$
291.9(2)	2399.6	$16^- \rightarrow 15^-$	3.06(7)	1.46(10)[d]	–	$M1+E2$
293.1(1)	293.1	$8^- \rightarrow 7^+$	100.0(4)	1.69(3)[b]	0.07(2)	$E1$
322.2(1)	3483.0	$19^{(-)} \rightarrow 18^{(-)}$	2.04(6)	1.13(9)[d]	–	$M1+E2$
327.7(2)	3213.8	$19^- \rightarrow 18^-$	3.37(5)	1.71(23)[b]	−0.25(6)	$M1$
373.8(2)	708.4	$11^- \rightarrow 9^-$	1.17(4)	0.95(14)[b]	–	$E2$
376.9(1)	3590.7	$20^- \rightarrow 19^-$	1.91(5)	1.67(21)[b]	−0.22(8)	$M1$
381.3(2)	4079.8	$(21^-) \rightarrow 20^{(-)}$	0.40(4)	–	–	–
403.5(1)	1356.7	$13^- \rightarrow 12^-$	12.67(19)	1.85(5)[d]	−0.05(2)	$M1+E2$
428.6(2)	4019.3	$21^- \rightarrow 20^-$	1.03(2)	1.69(37)[b]	–	$M1$
468.4(1)	2108.5	$15^- \rightarrow 14^-$	4.13(7)	1.50(7)[b]	−0.20(8)	$M1+E2$
478.3(2)	2877.6	$17^- \rightarrow 16^-$	1.70(3)	1.73(24)[b]	−0.13(10)	$M1+E2$
523.1(1)	953.2	$12^- \rightarrow 10^-$	11.87(18)	0.68(2)[d]	0.08(3)	$E2$
648.3(1)	1356.7	$13^- \rightarrow 11^-$	5.42(8)	0.65(4)[d]	0.39(5)	$E2$
686.7(1)	1640.0	$14^- \rightarrow 12^-$	13.62(20)	0.58(2)[d]	0.08(4)	$E2$
725.8(3)	3125.5	$18^- \rightarrow 16^-$	2.27(6)	0.57(6)[d]	–	$E2$
751.8(2)	2108.5	$15^- \rightarrow 13^-$	3.80(6)	0.54(4)[d]	0.27(8)	$E2$
759.5(2)	2399.6	$16^- \rightarrow 14^-$	10.84(24)	1.03(14)[e]	0.30(10)	$E2$
761.1(2)	3160.8	$18^{(-)} \rightarrow 16^-$	10.23(43)	0.58(9)[f]	–	$E2$
769.1(2)	2877.6	$17^- \rightarrow 15^-$	3.87(6)	0.68(3)[d]	0.07(4)	$E2$
876.4(1)	2516.4	$16^- \rightarrow 14^-$	6.90(11)	0.67(4)[d]	0.11(3)	$E2$

[a]Relative γ-ray intensities normalized to 100 for the 293.1-keV γ ray.
[b]From the 686.7-keV ($E2$) DCO gate.
[c]From the 648.3-keV ($E2$) DCO gate.
[d]From the 293.1-keV ($E1$) DCO gate.
[e]From the 725.8-keV ($E2$) DCO gate.
[f]From the 468.4-keV ($M1$) DCO gate.

been assumed to assign the parity of band B2, tentatively, as negative. The $M2$ character for the 761-keV transition could not, however, be ruled out and, hence, the parity of band B2 could be positive as well. A lifetime measurement of the $18^{(-)}$ state is necessary to overcome this ambiguity. The Weisskopf estimate of the half-lives corresponding to $E2$ and $M2$ character of this transition would be $\sim$ 50 ps and $\sim$5 ns, respectively. In the present work, we could not distinguish these two half-lives.

The 876-keV γ ray has been observed in the double-gated spectrum in Fig. 2(a) but not in the double-gated spectrum in Fig. 2(b) or 2(c). This γ ray was observed with any combination of double gates below the 1640-keV level but was not observed with any γ ray above this level. This indicates that the 876-keV γ ray must decay to the 14^- state of band B1. The cascade of γ rays in band B3 has been observed in Fig. 2(a). A sum of double-gated spectra, constructed from the combination of the 687-, 876-, 163-, 207, and 377-keV γ rays, is shown in Fig. 2(d). This spectrum clearly shows the 163-, 207-, 328-, 377-, and 429-keV γ rays belonging to this band. The $E2$ nature of the 876-keV γ ray is evident from its DCO and IPDCO ratios. Therefore, the bandhead of band B3 has been assigned as 16^-. The ordering of the γ rays in this band are based on their total intensities. However, since the crossover $E2$ transitions in this band were not observed, the ordering of the levels may be considered as somewhat tentative. The spins and parities of the states in this band are assigned from the measured DCO and the IPDCO ratios of the γ-ray transitions, wherever possible. The $R_{\rm DCO}$ values of these transitions are very close to the expected values for pure dipole transitions. The negative values obtained for the IPDCO ratios for the 328- and the 377-keV transitions, together with their $R_{\rm DCO}$ values, give clear evidence that they are predominantly $M1$ in nature. Since the other γ rays are in-band with the 328- and the 377-keV $M1$ transitions, we have assigned $M1$ nature for all the γ rays in this band.

IV. DISCUSSION

The high spin band structure in ^{194}Tl, obtained in the present work, can be discussed in the light of the neighboring isotopes. Ground-state band structures in the odd-odd Tl isotopes in the $A \sim 190$ region are similar to band B1 in ^{194}Tl. ^{190}Tl and ^{198}Tl are the other two isotopes for which definite excitation energies, spins, and parities are known for this band. However, it is interesting that the structure of this band in these two nuclei has been interpreted differently. In ^{190}Tl, this band was interpreted with oblate deformation [11] while in ^{198}Tl a possible chiral structure has been reported with triaxial deformation [17]. We have compared different properties of the ground-state band in the odd-odd Tl isotopes and have shown that they look very similar.

The configurations of the first few excited states in ^{194}Tl can be explained by the following arguments. The ground state of the odd-A Tl isotopes are $1/2^+$, corresponding to the $3s_{1/2}$ orbital near the proton Fermi level. In the isotone ^{193}Hg, the experimentally observed $5/2^-$ and $13/2^+$ states lie very close (within 40 and 141 keV, respectively) to the $3/2^-$ ground state [32]. These states correspond to the $f_{5/2}$, $i_{13/2}$, and $p_{3/2}$ orbitals, respectively, near the neutron Fermi level. Correspondingly, the configurations of the ground state (2^-) and the 7^+ isomeric state in the odd-odd ^{194}Tl nucleus have been attributed to $\pi s_{1/2} \otimes \nu p_{3/2}$ and $\pi s_{1/2} \otimes \nu i_{13/2}$ configurations, respectively. The 8^- state, at an excitation energy of 293 keV in this nucleus, has been interpreted as the bandhead of the $\pi h_{9/2} \otimes \nu i_{13/2}$ configuration [13]. These orbitals lie near the proton and the neutron Fermi levels of ^{194}Tl for an oblate deformation. The excitation energies of the 9^-, 10^-, and 11^- states in this band for ^{190,194,198}Tl nuclei are shown in Fig. 6, with respect to the excitation energy of the 7^+ isomeric state. It can be seen that the energies of these states increase smoothly with mass number A, as expected.

The alignment (i_x) for band B1 in ^{194}Tl is shown in Fig. 7 as a function of the rotational frequency $\hbar\omega$. The alignments for the neighboring odd-A nuclei ^{193}Tl and ^{193}Hg are also shown in Fig. 7, which have been deduced from the corresponding level schemes reported by Reviol *et al.* [33] and Hubel *et al.* [10], respectively. It can be seen that the band in ^{194}Tl has an initial alignment of about $5\hbar$. This value is in good agreement with the value obtained from the initial alignments of the neighboring odd-A nuclei using the additivity rule [34,35]. There is a gain in alignment of about $5\hbar$ at a rotational frequency of $\hbar\omega \sim 0.34$ MeV, which is similar to what is seen in ^{190}Tl and ^{198}Tl. The similarity between these odd-odd Tl isotopes is also reflected in their kinetic moments of inertia ($J^{(1)}$) values, as shown in Fig. 8. This indicates similar deformation in these nuclei. The particle alignments in these isotopes are also taking place at about the same frequency. In the present work, band B1 in ^{194}Tl could be extended just beyond the band crossing at $\hbar\omega_c \sim 0.34$ MeV.

The band-crossing phenomena in the odd-odd Tl isotopes can be understood from the band crossings in the even-even core of Hg isotopes and the band crossings in the odd-A Tl isotopes. In ^{192}Hg [10], the first two observed band crossings, at $\hbar\omega_{c1} \sim 0.210$ MeV and at $\hbar\omega_{c2} \sim 0.362$ MeV, were interpreted as due to the alignments of the $i_{13/2}$ neutrons (G $\rightarrow$ AB and AB $\rightarrow$ ABCD crossing, following the nomenclature of Hubel *et al.* [10]). The alignment of the protons takes place at even higher frequencies. The band crossings in the odd-Z ^{193}Tl

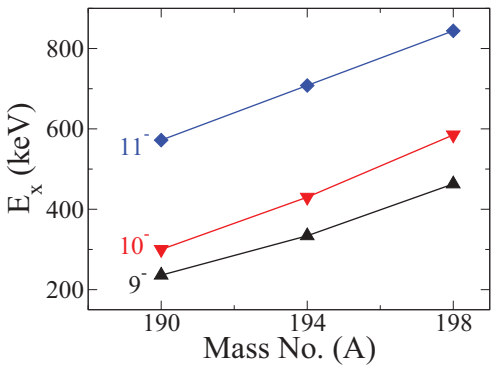

FIG. 6. (Color online) Excitation energies of the 9^-, 10^-, and 11^- states in odd-odd isotopes of Tl as a function of mass number A. Only the data for those isotopes for which the definite excitation energies are known with respect to the 7^+ isomeric state are plotted.

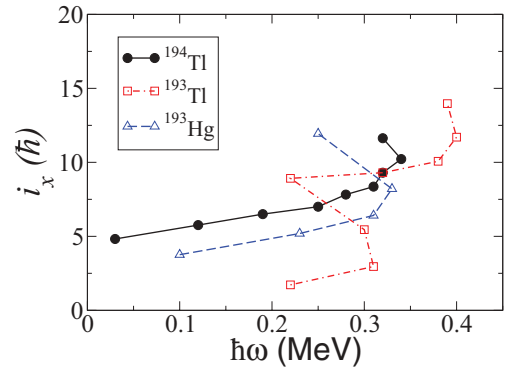

FIG. 7. (Color online) Experimental alignments (i_x) as a function of the rotational frequency ($\hbar\omega$) for the $\pi h_{9/2}$ band in ^{193}Tl [33], the $\nu i_{13/2}$ band in ^{193}Hg [10], and band B1 in ^{194}Tl. The Harris reference parameters are chosen to be $J_0 = 8.0\hbar^2$ MeV^{-1} and $J_1 = 40\hbar^4$ MeV^{-3}.

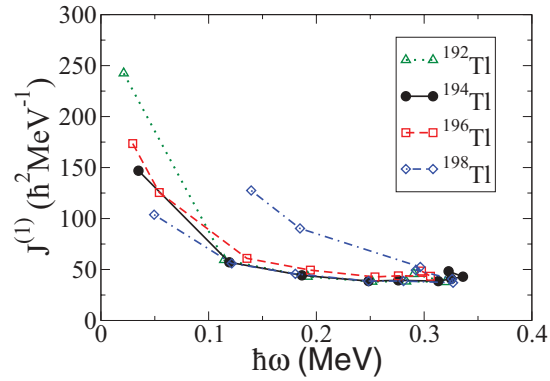

FIG. 8. (Color online) Experimental values of the moments of inertia $J^{(1)}$ as a function of the rotational frequency ($\hbar\omega$) for band B1 in ^{194}Tl compared with similar bands in ^{192,196,198}Tl.

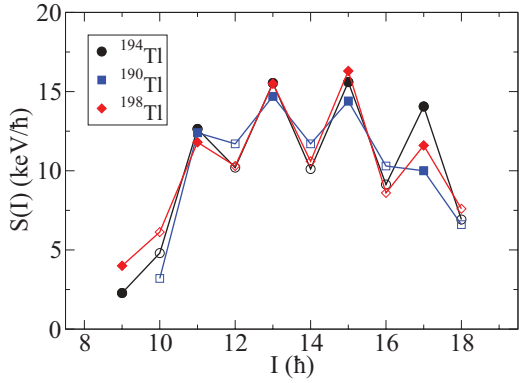

FIG. 9. (Color online) Staggering, $S(I) = [E(I) - E(I-1)]/2I$, plots as a function of spin (I) for the negative-parity yrast bands in ^{194}Tl along with those in ^{190,198}Tl.

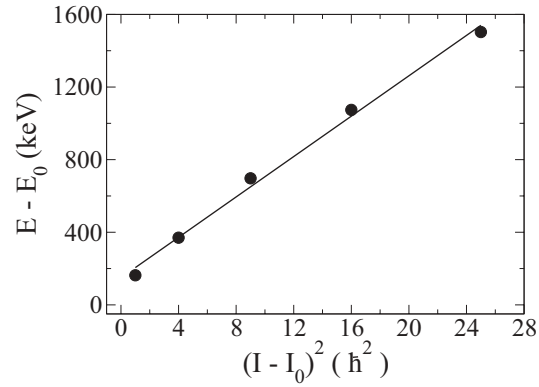

FIG. 10. Relative energy (E) vs spin (I) curve for band B3 built on the 16^- bandhead. E_0 and I_0 are the bandhead energy and spin, respectively. The fitted curve is shown by the solid lines (see text for details).

nucleus, in which the first proton crossing is blocked, were also interpreted as due to the alignments of the same $i_{13/2}$ neutrons. The crossing frequency of $\hbar\omega_c \sim 0.34$ MeV in ^{194}Tl agrees well with the $\hbar\omega_{c2}$ value in ^{192}Hg. Therefore, the observed band crossing in doubly odd ^{194}Tl may be attributed to the alignment of a pair of neutrons in the $i_{13/2}$ orbital. The similarity and the systematic trend of the observed AB $\rightarrow$ ABCD crossing frequencies for ^{190}Hg ($\hbar\omega_{c2} \sim 0.352$ MeV), ^{192}Hg ($\hbar\omega_{c2} \sim 0.362$ MeV), and ^{194}Hg ($\hbar\omega_{c2} \sim 0.348$ MeV) [10] are also in good agreement with the crossing frequencies of ^{192}Tl ($\hbar\omega_c \sim 0.32$ MeV), ^{194}Tl ($\hbar\omega_c \sim 0.34$ MeV), and ^{196}Tl ($\hbar\omega_c \sim 0.31$ MeV).

A low-spin signature inversion has been observed in the rotational bands in odd-odd nuclei in various mass regions, involving high-j configurations. In particular, the signature inversion has been reported for the prolate deformed odd-odd nuclei in the rare-earth region with a $\pi h_{9/2} \otimes \nu i_{13/2}$ configuration [36]. In the $A \sim 190$ region, the low-spin signature inversion for a band associated with an oblate $\pi h_{9/2} \otimes \nu i_{13/2}$ configuration has been reported in ^{190}Tl [11]. In the present work, a similar signature inversion has also been observed in ^{194}Tl. The signature inversion in a band can be identified experimentally in the plot of energy staggering, defined by $S(I) = [E(I) - E(I-1)]/2I$, where $E(I)$ is the energy of the state with spin I, as a function of the spin. This energy staggering has been plotted in Fig. 9 for the negative-parity yrast band of ^{194}Tl along with those for ^{190,198}Tl. The staggering plots of these three nuclei show remarkably similar behavior with low-spin signature inversion at the same spin value of $11\hbar$. A J-dependent residual p-n interaction was used to interpret the signature inversion in ^{190}Tl [11]. The similarity in the staggering plots suggests that the residual p-n interaction remains almost unchanged for the heavier odd-odd isotopes of ^{194,198}Tl.

The similarities in the band-crossing frequencies, the moments of inertia, the signature inversion, and the staggering plots for the above three nuclei suggest that the high spin properties of the ground-state band in all the odd-odd Tl isotopes in the $A \sim 190$ region are very similar and, therefore, they are expected to have similar structure. In the present work, we have not observed any indication of a chiral side band in ^{194}Tl, unlike in ^{198}Tl.

Band B3 in ^{194}Tl is a negative-parity band with a bandhead spin of $16\hbar$ at an excitation energy of 2.5 MeV. This band has been extended up to $21\hbar$ with predominantly $M1$ transitions. No $E2$ crossover transitions could be observed in this band. Band B3 lies at an energy which is somewhat higher than the crossing of the two- and four-quasiparticle configurations of band B1. Therefore, band B3 seems to be a six-quasiparticle band with two more protons in the $\pi h_{9/2}$ and $\pi s_{1/2}$ orbitals. The configuration of band B3 could, therefore, be assigned as $\pi h_{9/2}^2 s_{1/2}^{-1} \otimes \nu i_{13/2}^{-2} p_{3/2}$. The respective proton and neutron orbitals constitute the two-quasiparticle states in this nucleus at the lower excitation energies (2^- state, 7^+ state, and the 8^- bandhead of band B1). The experimental initial aligned angular momentum of $7\hbar$, deduced for this band, is consistent with the above configuration. The particle-hole configuration of this band with proton particles in high-j, high-Ω orbitals and neutron holes in high-j, low-Ω orbitals (for an oblate deformation) is favorable for magnetic rotation (MR) and, therefore, the excited states in this band may be generated by the shears mechanism. This band, with three particle-hole pairs, seems to follow the same general features of MR bands [19,37]. For the MR bands, the level energies (E) and the spin (I) in the band follow the pattern $E - E_0 \sim A(I - I_0)^2$, where E_0 and I_0 are the energy and the spin of the bandhead, respectively. The plot of $E - E_0$ versus $(I - I_0)^2$ for this band is shown in Fig. 10. The solid line is the fit of the data using the above relation. The good agreement of the data with the fitted curve in this plot clearly indicates that band B3 closely follows the above relation. By considering a higher limit of the intensity of the unobserved crossover $E2$ transitions as the level of the background in our data, the lower limit of the $B(M1)/B(E2)$ ratio has been estimated to be $>28\ \mu^2/(e\,\mathrm{b})^2$. This compares well with the typical value of $\geqslant 20\ \mu^2/(e\,\mathrm{b})^2$ for an MR band. The dynamic moment of inertia $J^{(2)} \sim 24\hbar^2\,\mathrm{MeV}^{-1}$ obtained for this band is also within the typical value of $J^{(2)} \sim 10$–$25\hbar^2\,\mathrm{MeV}^{-1}$ for an MR band. All these indicate that band B3 is, most likely, an MR band.

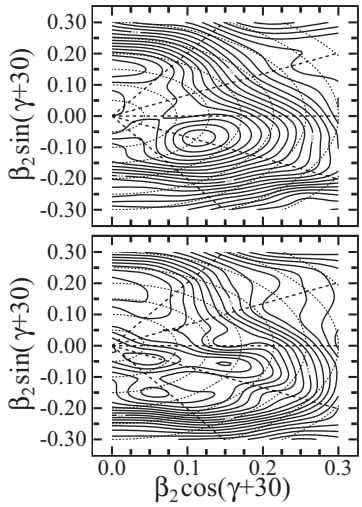

FIG. 11. Contour plots of the total Routhian surfaces in the β_2-γ deformation mesh for the configurations of bands B1 (top) and B3 (bottom) in ^{194}Tl at rotational frequencies $\hbar\omega = 0.11$ and 0.16 MeV, respectively. The contours are 400 keV apart.

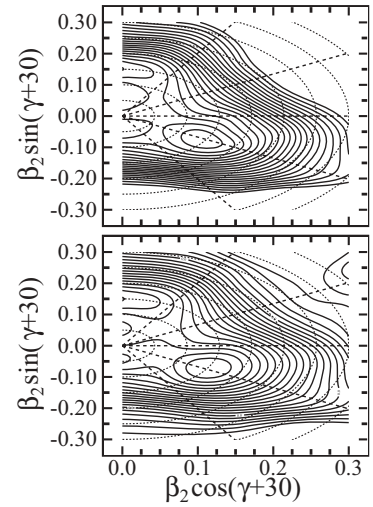

FIG. 12. Same as Fig. 11 but for ^{196}Tl (bottom) and ^{198}Tl (top) for the same configuration as band B1 of ^{194}Tl.

The bandlike structure B2 lies at an excitation energy of 3.16 MeV with a bandhead spin of $18\hbar$. The parity of this band remains tentative and this band is also not well developed. Therefore, characterization of this band at this moment would be rather premature. However, from the systematics of the odd-A Tl nuclei, it appears that this band may be generated with an additional proton pair in the $i_{13/2}$ orbital with the four-quasiparticle configuration of band B1 above its band crossing.

A. TRS calculations

In order to get an idea about the shape of the Tl nuclei for different configurations, total Routhian surface (TRS) calculations have been performed, in the β_2-γ deformation mesh points, where β_2 and γ are the quadrupole deformation parameters, with minimization in the hexadecapole deformation β_4, for bands B1 and B3 in ^{194}Tl. The Hartee-Fock-Bogoliubov code of Nazarewicz *et al.* [38,39] was used for the calculations. A deformed Woods-Saxon potential and pairing interaction were used with the Strutinsky shell correction method. The procedure has been outlined in Refs. [40,41]. The contour plots of the TRSs are shown in Fig. 11 for the two-quasiparticle $\pi h_{9/2} \otimes \nu i_{13/2}$ configuration corresponding to band B1 (top panel) and for the six-quasiparticle $\pi h^2_{9/2} s^{-1}_{1/2} \otimes \nu i^{-2}_{13/2} p_{3/2}$ configuration corresponding to band B3 (bottom panel) in ^{194}Tl. These surfaces were calculated at rotational frequencies of $\hbar\omega = 0.11$ and 0.16 MeV, respectively. The plots clearly show minima in the TRS at an oblate deformation ($\gamma = 0^\circ$ is prolate and $\gamma = -60^\circ$ is oblate) with $\beta_2 \sim 0.15$ and $\gamma \sim -57^\circ$ for band B1 and a near spherical shape with $\beta_2 \sim 0.06$ and $\gamma \sim -80^\circ$ for band B3.

The surfaces calculated for the same two-quasiparticle configuration as in band B1 are shown in Fig. 12 for ^{196}Tl and for ^{198}Tl. The minima for these nuclei are also found to be at the oblate deformation with very similar β_2 values. The similarity in the calculated shapes for these nuclei corroborates well with the observed similarities in the properties of the $\pi h_{9/2} \otimes \nu i_{13/2}$ bands in odd-odd Tl nuclei. The oblate shapes in all these three nuclei are predicted to persist over a rotational frequency range up to the band crossing. After the band crossing, the shape of ^{194}Tl remains almost the same with deformation $\beta_2 \sim 0.13$ and $\gamma \sim -53^\circ$. The lack of quadrupole deformation calculated for band B3 in ^{194}Tl is consistent with the nonobservation of $E2$ transitions and the conjecture of this band being of MR nature.

The calculated quasiparticle Routhians for the protons ($Z = 81$) and the neutrons ($N = 113$) in ^{194}Tl are shown in the left and right panels, respectively, of Fig. 13 for the deformation parameters $\beta_2 = 0.15$, $\gamma = -57^\circ$, and $\beta_4 = -0.02$ corresponding to the minimum in the TRS in Fig. 11. These calculations predict the first neutron pair alignment (AB crossing) at around $\hbar\omega \sim 0.14$ MeV and a second one (CD crossing) around $\hbar\omega \sim 0.23$ MeV. These are in good

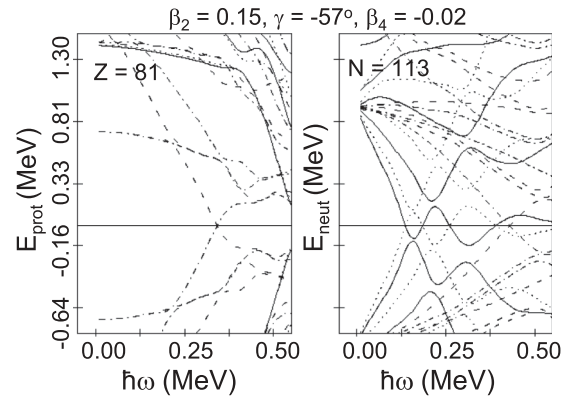

FIG. 13. Calculated quasiparticle Routhians as a function of rotational frequency $\hbar\omega$ for $Z = 81$ (left) and $N = 113$ (right) for the deformation $\beta_2 = 0.15$, $\gamma = -57^\circ$, and $\beta_4 = -0.02$. The quantum numbers (π, α) of the levels are drawn as follows: solid line $(+, +1/2)$, dotted line $(+, -1/2)$, dash-dotted line $(-, +1/2)$, and dashed line $(-, -1/2)$.

agreement with the values obtained using similar calculations for ^{193}Tl by Reviol *et al.* [33]. The same nomenclature as that of Ref. [33] has been used in our calculations to label the quasiparticle levels. The observed band crossings at $\hbar\omega \sim 0.28$ MeV and at $\hbar\omega \sim 0.37$ MeV in ^{193}Tl were identified as due to the first and second neutron pair alignments by Reviol *et al.* The calculated crossing frequencies, however, are found to underpredict both the experimental crossing frequencies by the same amount, and this discrepancy was attributed to the fact that the core deformation is not stiff, as assumed in these calculations. In addition to the first proton pair alignment, as in ^{193}Tl, the first neutron pair alignment is also blocked in the odd-odd nucleus ^{194}Tl. Therefore, the experimental band crossing in ^{194}Tl, observed at a rotational frequency of $\hbar\omega \sim 0.34$ MeV, is due to the second neutron pair alignment. This value of the crossing frequency is in fairly good agreement with the observed second crossing in ^{193}Tl but at a slightly lower frequency. The experimental crossing frequency in ^{194}Tl is lowered by 0.03 MeV compared to the second crossing in ^{193}Tl. This difference of the experimental crossing frequencies in these two nuclei is reproduced well in the calculated second neutron pair alignment frequencies for ^{194}Tl ($\hbar\omega \sim 0.23$ MeV) obtained in our calculation and that for ^{193}Tl ($\hbar\omega \sim 0.26$ MeV) as obtained by Reviol *et al.* [33].

B. Semiclassical calculations for band B3

To investigate the shears mechanism of band B3, we use the semiclassical approach of Macchiavelli and coworkers [19,42,43]. This is based on a schematic model of the coupling of two long j vectors (j_π and j_ν), corresponding to the proton and the neutron parts of the angular momenta. The aim is to extract information on the effective interaction between the nucleons which are involved in the shears mechanism. In this model, the shears angle (θ) between the two j vectors is an important variable which can be derived using the equation

$$\cos\theta = \frac{I^2 - {j_\pi}^2 - {j_\nu}^2}{2\, j_\pi\, j_\nu}, \tag{3}$$

where I is the total angular momentum. Given the $\boldsymbol{j}_\pi$ and $\boldsymbol{j}_\nu$ values of $8.5\hbar$ and $13.5\hbar$, respectively, for the proposed $\pi h_{9/2}^2 s_{1/2}^{-1} \otimes \nu i_{13/2}^{-2} p_{3/2}$ configuration of band B3, the bandhead spin is calculated to be $16\hbar$, if perpendicular coupling is assumed. This is in excellent agreement with the observed spin of the bandhead of this band. The maximum spin for this configuration has been calculated as $22^-\hbar$, corresponding to $\theta = 0^\circ$, which is again consistent with the highest spin observed for this band in the present work. Therefore, the angular momentum along the entire range of the band is, most likely, generated through the shears mechanism. The good agreement of the initial and the final spin values of this band with the calculated ones implies that the spins are generated solely by the shears mechanism with very little or no contribution from the rotation of the core. This fact is, again, corroborated well by the small quadrupole deformation obtained for this band in the TRS calculations.

According to the prescription of Macchiavelli *et al.* [42], the excitation energies of the states in shears bands correspond

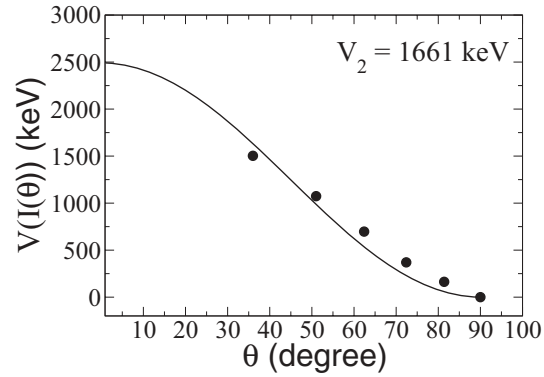

FIG. 14. The effective interaction between the angular momentum vectors, j_π and j_ν, as a function of shears angle θ for band B3 in ^{194}Tl as obtained in a semiclassical formalism.

to the change in the potential energy because of the recoupling of the angular momenta of the shears. The excitation energies of the states in the band, with respect to the bandhead energy, can be written as

$$V(I(\theta)) = E_I - E_b = (3/2)V_2\, \cos^2\theta_I, \tag{4}$$

where E_I is the energy of the level with angular momentum I, θ_I is the corresponding shears angle as given in Eq. (3), E_b is the bandhead energy, and V_2 is the strength of the interaction between the blades of the shears. Therefore, V_2 can be calculated by using the experimentally observed energy levels of the shears band. In Fig. 14, $V(I(\theta))$ is plotted as a function of θ. V_2 has been extracted from this plot by a fit of Eq. (4). The fitted curve is shown as the solid line in Fig. 14. The extracted value of V_2 comes out to be 1661 keV, which corresponds to an effective interaction of 332 keV per particle-hole pair for the suggested configuration of band B3. This value of the effective interaction is in good agreement with the typical value of ~ 300 keV observed for the MR bands in Pb nuclei in this region [44].

V. CONCLUSION

Gamma-ray spectroscopy of the high spin states in the odd-odd nucleus ^{194}Tl has been studied in the fusion-evaporation reaction using ^{185,187}Re targets with a ^{13}C beam at 75 MeV. A new and improved level scheme of ^{194}Tl is presented in this work which includes 19 new γ-ray transitions. The DCO ratio and the polarization asymmetry ratio measurements have been performed to assign the spins and parities of the levels. The $\pi h_{9/2} \otimes \nu i_{13/2}$ band (B1) in this nucleus has been extended just beyond the band crossing and up to a spin of $18^-\hbar$. The uncertainties in the excitation energies and the spins in this band have been removed. The moment of inertia, alignment, energy staggering, and signature inversion of this band have been found to be very similar to its neighboring odd-odd isotopes. The TRS calculations predict similar structure for these nuclei and support the observed similarity. We have not found any indication of a chiral doublet band structure in ^{194}Tl, unlike the one reported for ^{198}Tl. The observed band crossing in ^{194}Tl could also be understood from the band crossing in the

neighboring odd-A nuclei with oblate deformation. Therefore, it needs further experimental and theoretical investigation to understand the possible change, if any, in the structure of this two-quasiparticle band in ^{198}Tl. Two new side bands (B2 and B3) have been observed in this work in ^{194}Tl. Six-quasiparticle configurations for these bands have been suggested. A near spherical shape is predicted by the TRS calculations for band B3 and is consistent with the suggested MR nature of this band. This band has been discussed in the framework of a semiclassical approach. The observed bandhead spin and the range of the spin values of this band are in agreement with such calculations. However, to get a microscopic understanding of this band, tilted axis cranking calculations are needed.

ACKNOWLEDGMENTS

The untiring efforts of the operators and support staff at the BARC-TIFR Pelletron are acknowledged for providing a good beam of ^{13}C. The authors gratefully acknowledge the efforts of R. G. Pillay and V. Nanal for the smooth running of the experiment and illuminating discussions. The help of the INGA community in setting up the array and its associated electronics is gratefully acknowledged.

[1] R. M. Diamond and F. S. Stephens, Nucl. Phys. A **45**, 632 (1963).
[2] V. T. Gritsyna and H. H. Foster, Nucl. Phys. A **61**, 129 (1965).
[3] J. O. Newton, S. D. Cirilov, F. S. Stephens, and R. M. Diamond, Nucl. Phys. A **148**, 593 (1970).
[4] J. O. Newton, F. S. Stephens, and R. M. Diamond, Nucl. Phys. A **236**, 225 (1974).
[5] R. M. Lieder *et al.*, Nucl. Phys. A **299**, 255 (1978).
[6] A. J. Kreiner *et al.*, Phys. Rev. C **38**, 2674 (1988).
[7] M. G. Porquet *et al.*, Phys. Rev. C **44**, 2445 (1991).
[8] W. Reviol *et al.*, Phys. Scr., T **56**, 167 (1995).
[9] I. G. Bearden *et al.*, Nucl. Phys. A **576**, 441 (1994).
[10] H. Hübel *et al.*, Nucl. Phys. A **453**, 316 (1986).
[11] C. Y. Xie *et al.*, Phys. Rev. C **72**, 044302 (2005).
[12] A. J. Kreiner, A. Filevich, G. Garcia Bermudez, M. A. J. Mariscotti, C. Baktash, E. der Mateosian, and P. Thieberger, Phys. Rev. C **21**, 933 (1980).
[13] A. J. Kreiner, M. Fenzl, U. Heim, and W. Kutschera, Phys. Rev. C **20**, 2205 (1979).
[14] A. J. Kreiner *et al.*, Nucl. Phys. A **308**, 147 (1978).
[15] A. J. Kreiner *et al.*, Nucl. Phys. A **282**, 243 (1977).
[16] A. J. Kreiner, M. A. J. Mariscotti, C. Baktash, E. der Mateosian, and P. Thieberger, Phys. Rev. C **23**, 748 (1981).
[17] E. A. Lawrie *et al.*, Phys. Rev. C **78**, 021305(R) (2008).
[18] H. Hübel, Prog. Part. Nucl. Phys. **54**, 1 (2005).
[19] R. M. Clark and A. O. Macchiavelli, Annu. Rev. Nucl. Part. Sci. **50**, 1 (2000).
[20] F. Azaiez *et al.*, Z. Phys. A **336**, 243 (1990).
[21] F. Azaiez *et al.*, Phys. Rev. Lett. **66**, 1030 (1991).
[22] P. L. Masiteng *et al.*, Acta Phys. Pol. B **40**, 657 (2009).
[23] H. Tan *et al.*, in *Nuclear Science Symposium Conference Record 2008* (IEEE, Washington, DC, 2008), p. 3196.
[24] R. Palit *et al.*, Nucl. Instrum. Methods Phys. Res., Sect. A **680**, 90 (2012).
[25] R. Palit, AIP Conf. Proc. **1336**, 573 (2011).
[26] D. C. Radford, Nucl. Instrum. Methods Phys. Res., Sect. A **361**, 297 (1995).
[27] A. Krämer-Flecken *et al.*, Nucl. Instrum. Methods Phys. Res., Sect. A **275**, 333 (1989).
[28] E. S. Macias *et al.*, Comput. Phys. Commun. **11**, 75 (1976).
[29] K. Starosta *et al.*, Nucl. Instrum. Methods Phys. Res., Sect. A **423**, 16 (1999).
[30] Ch. Droste *et al.*, Nucl. Instrum. Methods Phys. Res., Sect. A **378**, 518 (1996).
[31] B. Singh, Nucl. Data Sheets **107**, 1531 (2006).
[32] E. Achterberg *et al.*, Nucl. Data Sheets **107**, 1 (2006).
[33] W. Reviol *et al.*, Nucl. Phys. A **548**, 331 (1992).
[34] R. Bengtsson and S. Frauendorf, Nucl. Phys. A **327**, 139 (1979).
[35] R. Bengtsson and S. Frauendorf, Nucl. Phys. A **314**, 27 (1979).
[36] I. Hamamoto, Phys. Lett. B **235**, 221 (1990).
[37] A. K. Jain *et al.*, Pramana **75**, 51 (2010).
[38] W. Nazarewicz *et al.*, Nucl. Phys. A **512**, 61 (1990).
[39] W. Nazarewicz *et al.*, Nucl. Phys. A **435**, 397 (1985).
[40] G. Mukherjee, H. C. Jain, R. Palit, P. K. Joshi, S. D. Paul, and S. Nagraj, Phys. Rev. C **64**, 034316 (2001).
[41] G. Mukherjee *et al.*, Nucl. Phys. A **829**, 137 (2009).
[42] A. O. Macchiavelli *et al.*, Phys. Rev. C **57**, R1073 (1998).
[43] A. O. Macchiavelli *et al.*, Phys. Rev. C **58**, R621 (1998).
[44] R. M. Clark and A. O. Macchiavelli, Nucl. Phys. A **682**, 415c (2001).